Femtosecond-Long Pulse-Based Modulation for Terahertz Band Communication in Nanonetworks

Josep Miquel Jornet, *Member, IEEE,* and Ian F. Akyildiz, *Fellow, IEEE*

***Abstract*—Nanonetworks consist of nano-sized communicating devices which are able to perform simple tasks at the nanoscale. Nanonetworks are the enabling technology of long-awaited applications such as advanced health monitoring systems or high-performance distributed nano-computing architectures. The peculiarities of novel plasmonic nano-transceivers and nano-antennas, which operate in the Terahertz Band (0.1-10 THz), require the development of tailored communication schemes for nanonetworks. In this paper, a modulation and channel access scheme for nanonetworks in the Terahertz Band is developed. The proposed technique is based on the transmission of one-hundred-femtosecond-long pulses by following an asymmetric On-Off Keying modulation Spread in Time (TS-OOK). The performance of TS-OOK is evaluated in terms of the achievable information rate in the single-user and the multi-user cases. An accurate Terahertz Band channel model, validated by COMSOL simulation, is used, and novel stochastic models for the molecular absorption noise in the Terahertz Band and for the multi-user interference in TS-OOK are developed. The results show that the proposed modulation can support a very large number of nano-devices simultaneously transmitting at multiple Gigabits-per-second and up to Terabits-per-second, depending on the modulation parameters and the network conditions.**

***Index Terms*—Nanonetworks, terahertz band, pulse-based communication, modulation.**

I. Introduction

NANOTECHNOLOGY is providing a new set of tools to the engineering community to design and manufacture nanoscale components, able to perform only specific tasks at the nanoscale, such as computing, data storing, sensing and actuation. The integration of several of these nano-components into a single entity will result in autonomous nano-devices. By means of communication, these nano-devices will be able to achieve complex tasks in a distributed manner. The resulting nanonetworks will enable new applications of nanotechnology in the biomedical, environmental and military fields.

One of the early applications of nanonetworks is in the field of nanosensing [2]. Nanosensors are nano-devices that take advantage of nanomaterials to detect new types of events at the nanoscale. For example, they can detect chemical compounds in very low concentrations (even a single molecule), and virus or harmful bacteria in very small populations. The size of an individual nanosensor is in the order of a few cubic micrometers, but their sensing range is limited to a few cubic micrometers as well. By means of communication, nanosensors will be able to transmit their information in a multi-hop fashion to a common sink. The resulting Wireless NanoSensor Networks (WNSNs) can be embedded for example in the fabric of our clothing to enable advanced health monitoring systems. Another application of nanonetworks is in the area of Wireless Network on Chip (WNoC) [3]. For example, wireless unicast, multicast and broadcast communication among nano-processors can drastically change the design principles of high-performance distributed computer architectures.

The communication requirements of nanonetworks widely change across applications. For example, in WNSNs, very high node densities, in the order of hundreds of nanosensors per square millimeter, are needed to overcome the limited sensing range of individual devices. In addition, different type of nanosensors might be interleaved to detect different types of chemical compounds, which results in up to thousands of nano-devices per square millimter. With an individual response time of multiple microseconds [2], the aggregated throughput could reach multiple Gigabits per second (Gbps). When it comes to WNoC, the processing speed of an individual core and the total number of cores determines the aggregated throughput. From [3], data rates in the order of hundreds of Gbps per core are common, and multi-core architectures with tens and hundreds of cores already exist. While not all the cores might need wireless links all the time, peak data rates in the order of Terabits per second (Tbps) need to be supported.

To date, the communication options for nano-devices are very limited. The miniaturization of a conventional metallic antenna to meet the size requirements of the nano-devices would impose the use of very high operating frequencies (hundreds of Terahertz). The available transmission bandwidth increases with the antenna resonant frequency, but so does the propagation loss. Due to the expectedly very limited power of nano-devices, the feasibility of nanonetworks would be compromised if this approach were followed. Alternatively, graphene, i.e., a one-atom-thick layer of carbon atoms in a honeycomb crystal lattice [4], has been proposed as the building material of novel plasmonic nano-antennas [5], [6]. These can efficiently operate at Terahertz Band frequencies (0.1-10 THz) [7], [8], [9], by exploiting the behavior of Surface Plasmon Polariton (SPP) waves. Nano-antennas are just tens of nanometers wide and few micrometers long, and can potentially be easily integrated in nano-devices.

Manuscript received May 30, 2013; revised November 4, 2013 and February 19, 2014. The editor coordinating the review of this paper and approving it for publication was M. Buehrer.

This work was supported by the U.S. National Science Foundation (NSF) under Grant No. CCF-1349828.

J. M. Jornet is with the Department of Electrical Engineering, University at Buffalo, The State University of New York, NY 14260, USA (e-mail: jmjornet@buffalo.edu).

I. F. Akyildiz is with the Broadband Wireless Networking Laboratory, School of Electrical and Computer Engineering, Georgia Institute of Technology, Atlanta, GA 30332, USA (e-mail: ian@ece.gatech.edu).

A preliminary version of this work was presented in [1].

Digital Object Identifier 10.1109/TCOMM.2014.033014.130403

In this same direction, compact Terahertz Band plasmonic signal generators and detectors are being developed [10], [11]. Contrary to classical Terahertz Band radiation sources, which usually require high power bulky devices and sophisticated cooling systems [12], solid-state Terahertz Band emitters can electronically excite SPP waves at Terahertz Band frequencies from a compact structure built on a High Electron Mobility Transistor (HEMT) based on semiconductor materials. However, for the time being, at room temperature, only very short pulses, just a hundred femtosecond long, can be generated, with a power of just a few μW per pulse. While this might not be enough for long range Terahertz Band communication, it opens the door to communication in nanonetworks.

The lack of nanoscale transceivers able to generate a carrier signal at Terahertz Band frequencies limits the feasibility of carrier-based modulations, and motivates the use of pulse-based communication schemes in nanonetworks. When size is not a constraint, carrier-based modulations can still be used, as shown in [13], [14], [15]. Pulse-based modulations have been widely used in very high speed communications systems such as Impulse Radio Ultra-Wide-Band (IR-UWB) [16] and free-space optical (FSO) systems [17]. However, the peculiarities of nano-transceivers and nano-antennas and the phenomena that affect the propagation of these very short pulses in the Terahertz Band requires a revision of common assumptions in pulse-based communications.

In this paper, we propose and analyze the performance of a pulse-based modulation and channel access scheme for nanonetworks in the Terahertz Band, which is based on the transmission of one-hundred-femtosecond-long pulses by following an asymmetric On-Off Keying modulation Spread in Time (TS-OOK). This scheme is tailored to the expected capabilities of Terahertz Band signal generators and detectors, and exploits the peculiarities of the Terahertz Band channel.

The main contributions of this paper are summarized as follows. First, in Sec. II, we revise the state of the art and highlight the peculiarities of Terahertz Band nanoscale signal generators and detectors, the impact of the nano-antenna in the transmission and in reception, as well as the channel effects and propagation phenomena in the Terahertz Band.

Second, in Sec. III, we propose TS-OOK as a modulation and channel access scheme for nanonetworks in the Terahertz Band and briefly describe its functioning in the single-user and the multi-user cases. Third, we analytically model the performance of TS-OOK in an interference-free scenario. For this, we develop a new stochastic model of noise in the Terahertz Band, and we use this model to analyze the maximum achievable information rate. The details on the noise model and information rate analysis are presented in Sec. IV.

Fourth, we extend our analysis on the performance of TS-OOK to the multi-user case. For this, we develop a stochastic model of multi-user interference in pulse-based communication in the Terahertz Band. This model considers a uniform distribution of nano-devices in space, which communicate in an asynchronous manner in an ad-hoc fashion and without a central coordinator. We then use this model to analytically investigate the achievable information rate in the presence of multi-user interference. Our analysis is treated in Sec. V.

Finally, we use COMSOL Multi-physics [18] to validate our models by mean of time-domain electromagnetic simulations, and we numerically investigate the achievable information rate for the two cases under study. Our results show that, despite its simplicity, when using TS-OOK, nanonetworks can support a very large number of nano-devices simultaneously transmitting at very high bit-rates, given that asymmetric source probability distributions are used to prioritize the transmission of silence. The achievable rates range from a few Gbps to a few Tbps, depending on the TS-OOK parameters and nano-device density. The details on our simulation and numerical analysis are presented in Sec. VI. We conclude the paper in Sec. VII.

II. Terahertz Band Pulse-based Systems

A. Signal Generation

Terahertz Band signal generators for communication among nano-devices must be i) compact, i.e., up to several hundreds of square nanometers or a few square micrometers at most; ii) fast, i.e., able to support modulation bandwidths of at least several GHz; iii) energy-efficient, and iv) preferably tunable.

Several technologies are being considered for the generation of Terahertz Band signals. For the time being, monolithic integrated circuits based on Silicon [19], Silicon Germanium [20], Indium Phosphide [21] and Gallium Nitride [22], have been demonstrated at frequencies between 0.1 and 1 THz. For higher frequency operation, photonic devices and, in particular, Quantum Cascade Lasers (QCLs) [12], are commonly utilized. QCLs can operate at frequencies above a few THz and can generate an average power up to a few mW. However, the need of an external laser for optical electron pumping and their size (at least several square millimeters) hamper the application of QCLs for communication in nanonetworks.

More recently, compact signal generators are being developed by using a single HEMT based on III-V compound semiconductors (e.g., Gallium Nitride) as well as graphene [10], [11]. In particular, it has been shown that SPP waves at Terahertz Band frequencies can be excited in the channel of a HEMT with nanometric gate length by means of either electrical or optical pumping. When a voltage is applied between the drain and the source of the HEMT, electrons are accelerated from the source to the drain. This sudden movement of electrons results in the excitation of a SPP wave due to the energy band-structure of the building material of the HEMT. At room temperature, however, the SPP waves are overdamped and only very short broadband incoherent SPP waves are generated. These resemble very short pulses, just several tens of femtoseconds long.

In our analysis, we model the generated signals as one-hundred-femtosecond-long Gaussian pulses. These type of pulses are already being used in several applications such as Terahertz imaging and biological spectroscopy [23]. The p.s.d. of these pulses has its main frequency components in the Terahertz Band. Pulses with a peak power of a few μW, i.e., with equivalent energies of just a few aJ (10^{-18}J), have been reported in the related literature [11]. An additional technology limitation at the generator is that pulses cannot be transmitted in a burst, but due to the relaxation time of SPP waves in the HEMT channel, need to be spread in time. In our analysis,

we consider the energy per pulse and the spreading between pulses as two technology parameters.

B. Signal Radiation

The resulting plasmonic signal can be then radiated by a Terahertz Band plasmonic nano-antenna, such as the designs proposed in [5], [6]. The radiated waveform depends on the antenna behavior in transmission. Contrary to classical narrow-band communication systems, and in-line with UWB systems, the antenna response cannot be modeled with a single gain, but the entire frequency response or the antenna impulse response are needed. Independently of the particular antenna design, from [24], [25], the radiated electromagnetic field is proportional to the first time derivative of the current density at the antenna surface. For this, we model the antenna impulse response in transmission h_{ant}^{T} as:

$$h_{ant}^{T}(t) = \frac{\partial}{\partial t} \int \boldsymbol{J}_{||}^{\delta}(t, \boldsymbol{r}')\, dV', \tag{1}$$

where t refers to time, V' stands for the volume occupied by the antenna, $\boldsymbol{J}_{||}^{\delta}$ (in units of [1/m^{2}s]) is the current distribution on the antenna due to an impulse input current $\delta(t)$ in the transverse direction relative to the observation direction, and $\boldsymbol{r}' = (x, y)$. The current distribution on the antenna $\boldsymbol{J}_{||}^{\delta}$ depends on the particular antenna design, and usually it can only be numerically obtained. At this stage, we keep our analysis general for any possible antenna. In our results, we utilize COMSOL Multi-physics to account for the impact of an electric point dipole in transmission. More details are provided in Sec. VI.

C. Signal Propagation

The propagation of the radiated pulses is determined by the Terahertz Band channel behavior. Existing channel models for lower frequency bands cannot be utilized at Terahertz Band frequencies, because they do not capture the peculiarities of this frequency range, such as the impact of molecular absorption on the signal propagation. In addition, the few existing Terahertz Band channel models [26], [27], [28] are aimed at characterizing only a fraction of the Terahertz Band (e.g., 300 GHz window) and usually over large propagation distances (several meters). However, in light of the limited transmission power of nano-devices and the broadband nature of the generated signals, there is a need to model the entire Terahertz Band for distances much below one meter.

In this direction, we have recently developed a channel model for Terahertz Band communications [29]. The main difference with other frequency bands comes from the molecular absorption loss. The absorption loss accounts for the attenuation that a propagating wave suffers because of molecular absorption, i.e., the process by which part of the wave energy is converted into internal kinetic energy to some of the molecules which are found in the channel. This loss depends on the signal frequency, the transmission distance and the concentration and the mixture of molecules encountered along the path. As a result, the Terahertz Band channel is highly frequency selective, specially when the concentration of molecules or the transmission distance are increased.

From [29], the Terahertz Band channel frequency response H_c is given by

$$H_c(f, d) = H_{spread}(f, d)\, H_{abs}(f, d), \tag{2}$$

where H_{spread} and H_{abs} refer to the spreading loss and the molecular absorption loss, respectively, and are given by

$$H_{spread}(f, d) = \left(\frac{1}{\sqrt{4\pi} d}\right) \exp\left(-\imath 2\pi f d/c\right) \tag{3}$$

$$H_{abs}(f, d) = \exp\left(-\frac{1}{2} k(f)\, d\right), \tag{4}$$

where f stands for frequency, d stands for distance, and k is the medium absorption coefficient, given by

$$k(f) = \sum_i \frac{p}{p_0} \frac{T_{STP}}{T} Q^i \sigma^i(f), \tag{5}$$

where p refers to the system pressure in Kelvin, p_0 is the reference pressure (1 atm), T_{STP} is the temperature at standard pressure (273.15 K), Q is the number of molecules per volume unit of gas i and σ^i is the absorption cross-section of gas i. More details on how to compute the molecular absorption cross-section σ can be found in [29].

The channel impulse response h_c is obtained by using the Inverse Fourier transform

$$h_c(t, d) = \mathcal{F}^{-1}\{H_c(f, d)\}. \tag{6}$$

This inverse Fourier Transform does not have an analytical expression. In our analysis, we will numerically compute the channel time response. As we describe in Sec. VI, we use COMSOL Multi-physics to validate this model by means of extensive time-domain simulations. In addition, this model can successfully reproduce existing measurements for the lower range of the Terahertz Band between 100 GHz and 1 THz, such as the values reported in [27].

There are additional propagation effects that might impact the received signal, such as multi-path propagation. A multi-path model for the Terahertz Band needs to account for the impact of molecular absorption, the reflection coefficient of common materials at Terahertz Band frequencies and the impact of diffused scattering on rough surfaces [30], amongst others. The few multi-path channel models existing to date [28] are mainly focused on the 300 GHz window, and a complete model for the entire Terahertz Band does not exist. As a result, we do not account for multi-path in this work.

D. Signal Reception

The signal at the receiver depends on the antenna impulse response in reception. From [24], [25], this is proportional to the time integral of the antenna impulse response in transmission. For this, we model the antenna impulse response in reception h_{ant}^{R} as:

$$h_{ant}^{R}(t) = \int_0^t h_{ant}^{T}(\tau)\, d\tau, \tag{7}$$

where t refers to time and h_{ant}^{T} is the antenna impulse response in transmission, given by (1). As before, the antenna impulse response in reception depends on the particular antenna, and can generally only numerically be obtained. In our results, we

utilize COMSOL Multi-physics to incorporate the impact of an electric point dipole antenna in reception.

The system impulse response, which captures the impact of the antenna in transmission, the propagation effects, and the impact of the antenna in reception, is finally given by:

$$h(t) = h_{ant}^{T}(t) * h_c(t) * h_{ant}^{R}(t). \quad (8)$$

In classical narrow-band systems, the impact of the antenna in transmission and in reception is usually captured by taking into account the following relation between the antenna directivity D and its effective area A_{eff} in reception:

$$D\lambda^2 = 4\pi A_{eff}, \quad (9)$$

where λ stands for the wavelength at the design center frequency of the system. It is relevant to note that both the directivity D and the effective area A_{eff} depend on the frequency themselves, and thus, the utilization of the aforementioned expression would be a narrow-band approximation. We do not follow this approach, and model instead the antenna impulse response in transmission and in reception numerically in COMSOL.

E. Signal Detection

Many technologies are being considered for the detection of Terahertz Band signals. Currently, the most developed solutions rely on bolometers [31] and Schottky diodes [32]. On the one hand, bolometric detectors are able to detect very low power signals and have a high modulation bandwidth (up to a few GHz). However, their low performance at room temperature and their size pose a major constraint for the nano-devices. Similarly, the detection systems based on Schottky diodes can operate at room temperature and exhibit a high modulation bandwidth (up to 10 GHz), but their size limits their integration with the rest of the nano-transceiver.

Alternatively, the same HEMT-based structure discussed in transmission, has been proposed for the detection of Terahertz Band signals [10], [11]. The injection of a plasmonic current in the channel of the HEMT results into electrons being pushed from the source to the drain. This effectively creates a voltage between the drain and the source. Recent works show how HEMT-based detectors provide excellent sensitivities with the intrinsic possibility of high-speed response (limited only by the read-out electronics impedance).

Similarly as in transmission, at room temperature, HEMT-based detectors can only measure the amplitude of the received signals, but not their phase. A sensitivity or noise equivalent power as low as 10 fW/$\sqrt{\text{Hz}}$ has been reported in [33]. For the time being, an accurate symbol detection model for one-hundred-femtosecond-long pulses is missing. A preliminary version of our ongoing work to develop a new symbol detection model can be found in [34]. In order to separate the impact of the symbol detection scheme on the system performance, we will consider an ideal matched filter in our analysis.

III. Time Spread On-Off Keying

In this section, we describe the proposed communication technique for nanonetworks, which serves both as a modulation scheme as well as a multiple access mechanism.

A. Modulation Definition

In light of the capabilities of nano-transceivers, we propose the use of TS-OOK for communication among nano-devices in the Terahertz Band. TS-OOK is based on the exchange of one-hundred-femtosecond-long pulses among nano-devices. The functioning of this communication scheme is as follows:

- *A logical "1" is transmitted by using a one-hundred-femtosecond-long pulse and a logical "0" is transmitted as silence*, i.e., the nano-device remains silent when a logical zero is transmitted. As discussed above, solid-state Terahertz Band transceivers are not expected to be able to accurately control the shape or phase of the transmitted pulses and, thus, a simple OOK modulation is used. To avoid the confusion between the transmission of silence and the no transmission, initialization preambles and constant-length packets can be used. After the detection of the preamble, silence is considered a logical "0".
- *The time between transmissions is fixed and much longer than the pulse duration.* Due to the nano-transceiver limitations above described, pulses or silences are not transmitted in a burst, but spread in time as in IR-UWB. By fixing the time between consecutive transmissions, after an initialization preamble, a nano-device does not need to continuously sense the channel, but it just waits for the next transmission. This scheme does not require tight synchronization among nano-devices all the time, but only selected nano-devices will be synchronized after the detection of the initialization preamble.

Under this scheme, the signal transmitted by a nano-device u, s_T^u is given by:

$$s_T^u(t) = \sum_{k=1}^{K} A_k^u p(t - kT_s - \tau^u) \quad (10)$$

where K is the number of symbols per packet, A_k^u refers to the amplitude of the k-th symbol transmitted by the nano-device u (either 0 or 1), p stands for a pulse with duration T_p, T_s refers to the time between consecutive transmissions, and τ^u is a random initial transmission delay. In general, the time between symbols is much longer than the time between pulses. Following the usual notation, we define $\beta = T_s/T_p \gg 1$.

The signal received by a nano-device j can be written as:

$$s_R^j(t) = \sum_{k=1}^{K} A_k^u p(t - kT_s - \tau^u) * h^{u,j}(t) + n_k^{u,j}(t) \quad (11)$$

where $h^{u,j}$ is the system impulse response between the nano-devices u and j, in (8), and depends on the specific medium conditions and the distance between the transmitter u and the receiver j. $n_k^{u,j}$ stands for the noise affecting the transmission of symbol k between u and j, described in Sec. IV-A.

B. Medium Sharing with TS-OOK

TS-OOK enables robust and concurrent communication among nano-devices. In the envisioned scenarios, nano-devices can start transmitting at any time without being synchronized or controlled by any type of network central entity. However, due to the fact that the time between transmissions T_s is much longer than the pulse duration T_p,

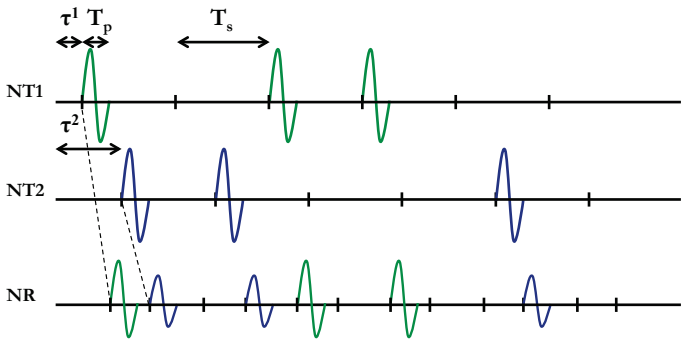

Fig. 1. TS-OOK illustration: top) First nano-device transmitting the sequence "101100"; middle) Second nano-device transmitting the sequence "110010"; bottom) Overlapped sequences at the receiver side.

several nano-devices can concurrently use the channel without necessarily affecting each other. In addition, the very short symbol duration T_p (i.e., ≈100 fs) makes collisions between symbols highly unlikely. Moreover, not all types of collisions are *harmful*. There are no collisions between silences, and collisions between pulses and silences are only harmful from the silence perspective, i.e., the intended receiver for the pulse will not notice any difference if silence is received at the same time. In any case, collisions may occur, creating multi-user interference.

The signal received by a nano-device j is given by:

$$s_R^j(t) = \sum_{u=1}^{U} \sum_{k=1}^{K} A_k^u p\left(t - kT_s - \tau^u\right) * h^{u,j}(t) + n_k^{u,j}(t) \tag{12}$$

where $U-1$ is the number of interfering nano-devices, K is the number of symbols per packet, A_k^u refers to the amplitude of the k-th symbol transmitted by the nano-device u (either 0 or 1), p stands for a pulse with duration T_p, T_s refers to the time between consecutive transmissions, τ^u is a random initial time, $h^{u,j}$ is the system impulse response between u and j in (8), and $n_k^{u,j}$ stands for the noise affecting the transmission of the k-th symbol between u and j.

In Fig. 1, we show an example of TS-OOK for the case in which two nano-devices are simultaneously transmitting different binary sequences to a third nano-device. The upper plot corresponds to the sequence "101100", which is transmitted by the first nano-device. A logical "1" is represented by the first derivative of a Gaussian pulse and a logical "0" is represented by silence. The time between symbols is T_s is very small for a real case but convenient for illustration purposes. This signal is propagated through the channel (thus, distorted and delayed). Similarly, the second plot shows the sequence transmitted by the second nano-device, "110010". This second transmitter is farther from the receiver than the first transmitter.

IV. Single-user Achievable Information Rate in TS-OOK

In this section, we develop a stochastic model of molecular absorption noise and analytically investigate the achievable information rate for TS-OOK in the single-user case.

A. Stochastic Model of Molecular Absorption Noise

To study the achievable information rate for TS-OOK in the single-user case, it is necessary to stochastically characterize the noise in the Terahertz Band. As described in [29], molecular absorption is one of the main noise sources at Terahertz Band frequencies. Excited molecules re-radiate out of phase part of the energy that they have previously absorbed. This is conventionally modeled as a noise factor [35]. Two main properties characterize this noise. On the one hand, molecular absorption noise is correlated to the transmitted signal. In particular, molecular absorption noise increases when transmitting, i.e., there is only background noise unless the molecules are irradiated [36]. On the other hand, different molecules resonate at different frequencies and, moreover, their resonance is not confined to a single frequency but spread over a narrow band. As a result, the power spectral density (p.s.d.) of the noise has several peaks in frequency.

The overall molecular absorption noise contribution at the receiver comes from a very large number of molecules, randomly positioned across the channel. By invoking the Central Limit Theorem, the total contribution at the receiver can be modeled as Gaussian. This is a common assumption, described also in [35], [36]. For a specific resonance v, this noise can be characterized by a Gaussian probability distribution with mean equal to zero and variance given by the noise power within the band of interest,

$$\mathcal{N}_v\left(\mu_v = 0, \sigma_v^2 = \int_B S_{N_v}(f)\, df\right), \tag{13}$$

where $S_{N_v}(f)$ refers to the p.s.d. of the molecular absorption noise created by the resonance v, and B stands for the receiver's equivalent noise bandwidth. By considering the different resonances from the same molecule as well as the resonances in different molecules to be independent, we can model the total molecular absorption noise also as additive Gaussian noise, with mean equal to zero and variance given by the addition of the noise power corresponding to each resonance, $\mathcal{N}\left(\mu = 0, \sigma^2 = \sum_v \sigma_v^2\right)$.

The variance of the molecular absorption noise can also be obtained by integrating the total noise p.s.d. over the receiver's noise equivalent bandwidth. The total molecular absorption noise p.s.d. S_{N_m} affecting the transmission of a symbol $m \in \{0,1\}$ is contributed by the background atmospheric noise p.s.d. S_{N^B} [35] and the self-induced noise p.s.d. $S_{N_m^X}$, which are defined as

$$S_{N_m}(f,d) = S_{N^B}(f) + S_{N_m^X}(f,d) \tag{14}$$

$$S_{N^B}(f) = \lim_{d\to\infty} k_B T_0 \left(1 - |H_{abs}(f,d)|^2\right) \left|H_{ant}^R(f)\right|^2 \tag{15}$$

$$S_{N_m^X}(f,d) = S_{X_m}(f) \left|H_{ant}^T(f)\right|^2 \left(1 - |H_{abs}(f,d)|^2\right) \cdot |H_{spread}(f,d)|^2 \left|H_{ant}^R(f)\right|^2, \tag{16}$$

where d refers to the transmission distance, f stands for the frequency, k_B is the Boltzmann constant, T_0 is the room temperature, H_{abs} is the molecular absorption loss given by (4), H_{spread} is the spreading loss given by (3), H_{ant}^R and H_{ant}^T are the antenna frequency response in reception and transmission,

respectively, which are obtained as the Fourier transform of (7) and (1), and S_{X_m} is the p.s.d. of the transmitted signal.

The term S_{N^B} takes into account that the background noise is i) generated from molecules that radiate for being at a temperature above 0 K, and ii) detected by an antenna in reception. The term $S_{N_m^X}$ takes into account that the induced noise is i) generated by the transmitted signal X_m, ii) spherically spread from the transmitting antenna, and iii) detected by an antenna in reception.

Finally, the total noise power at the receiver N_m when the symbol $m \in \{0,1\}$ is transmitted is given by

$$N_m(d) = \int_B S_{N_m}(f,d) \left|H_r(f)\right|^2 df, \tag{17}$$

where B is the receiver's noise equivalent bandwidth and H_r is the receiver's frequency response described in Sec. II.

In addition to the molecular absorption noise, there are other noise sources that can affect the achievable information rate in the proposed scheme, such as the electronic noise at the receiver. The noise factor at the receiver drastically depends on the specific device technology. However, a stochastic model for the electronic noise at the receiver is missing. In our analysis, we aim at obtaining an upper bound, independent of the transceiver technology. These results will be extended as stochastic noise models for the receiver are developed.

B. Analytical Study of the Single-user Information Rate

The maximum achievable information rate in bit/symbol IR_{u-sym} of a communication system for a specific modulation scheme is given by

$$IR_{u-sym} = \max_X \left\{H(X) - H(X|Y)\right\}, \tag{18}$$

where X refers to the source of information, Y refers to the output of the channel, $H(X)$ refers to the entropy of the source X, and $H(X|Y)$ stands for the conditional entropy of X given Y or the equivocation of the channel.

In our analysis, we consider the source of information X to be discrete, and the output signal of the transmitter s_T^u in (10), the channel response h in (8) and the molecular absorption noise n to be continuous. Under these considerations, the source X can be modeled as a discrete binary random variable. Therefore, the entropy of the source $H(X)$ is given by:

$$H(X) = -\sum_{m=0}^{1} p_X(x_m) \log_2 p_X(x_m), \tag{19}$$

where $p_X(x_m)$ refers to the probability of transmitting the symbol $m = \{0,1\}$, i.e., the probability to stay silent or to transmit a pulse, respectively.

The output Y of the channel can be modeled as a continuous random variable. In particular, the output of the transmitter is distorted by the channel h, and corrupted by the molecular absorption noise n. The only random component affecting the received signal is the molecular absorption noise.

By recalling the Mixed Bayes Rule and the Total Probability Theorem [37], the equivocation $H(X|Y)$ can be written in terms of the probability of the channel output Y given the input x_m, $f_Y(Y|X=x_m)$,

$$\begin{aligned} H(X|Y) = \int_y \sum_{m=0}^{1} f_Y(Y|X=x_m)\, p_X(x_m) \\ \cdot \log_2 \left(\frac{\sum_{n=0}^{1} f_Y(Y|X=x_n)\, p_X(x_n)}{f_Y(Y|X=x_m)\, p_X(x_m)} \right) dy. \end{aligned} \tag{20}$$

Based on the stochastic model of molecular absorption noise, the p.d.f. of the output of the system Y given the input $X = x_m$ can be written as:

$$f_Y(Y|X=x_m) = \frac{1}{\sqrt{2\pi N_m}} e^{-\frac{1}{2}\frac{(y-a_m)^2}{N_m}}, \tag{21}$$

where N_m stands for the total noise power associated to the transmitted symbol x_m and a_m refers to the amplitude of the received symbol, which is obtained by using the Terahertz Band system model described in Sec. II.

By combining (19), (20) and (21) in (18), the achievable information rate in bit/symbol can be written as (22). Finally, the maximum achievable information rate in bit/second is obtained by multiplying the rate in bit/symbol (22) by the rate at which symbols are transmitted, $R = 1/T_s = 1/(\beta T_p)$, where T_s is the time between symbols, T_p is the pulse length, and β is the ratio between them. If we assume that the $BT_p \approx 1$, where B stands for the channel bandwidth, the

$$\begin{aligned} IR_{u-sym} = \max_X \Bigg\{ & -\sum_{m=0}^{1} p_X(x_m) \log_2 p_X(x_m) - \int \sum_{m=0}^{1} \frac{1}{\sqrt{2\pi N_m}} e^{-\frac{1}{2}\frac{(y-a_m)^2}{N_m}} p_X(x_m) \\ & \cdot \log_2 \left(\sum_{n=0}^{1} \frac{p_X(x_n)}{p_X(x_m)} \sqrt{\frac{N_m}{N_n}} e^{-\frac{1}{2}\frac{(y-a_n)^2}{N_n} + \frac{1}{2}\frac{(y-a_m)^2}{N_m}} \right) dy \Bigg\} \\ = - \max_{p_X(x_0)} \Bigg\{ & \int \frac{p_X(x_0)}{\sqrt{2\pi N_0}} e^{-\frac{1}{2}\frac{y^2}{N_0}} \log_2 \left(p_X(x_0) \left(1 + \frac{1-p_X(x_0)}{p_X(x_0)} \sqrt{\frac{N_0}{N_1}} e^{-\frac{1}{2}\frac{y^2}{N_0} + \frac{1}{2}\frac{(y-a_1)^2}{N_1}} \right) \right) \\ & + \frac{1-p_X(x_0)}{\sqrt{2\pi N_1}} e^{-\frac{1}{2}\frac{(y-a_1)^2}{N_1}} \log_2 \left((1-p_X(x_0)) \left(1 + \frac{p_X(x_0)}{1-p_X(x_0)} \sqrt{\frac{N_1}{N_0}} e^{-\frac{1}{2}\frac{(y-a_1)^2}{N_1} + \frac{1}{2}\frac{y^2}{N_0}} \right) \right) dy \Bigg\}. \end{aligned} \tag{22}$$

rate in bit/second is given by:

$$IR_u = \frac{B}{\beta} IR_{u-sym}. \tag{23}$$

If $\beta = 1$, i.e., all the symbols (pulses or silences) are transmitted in a burst, and the maximum rate per nano-device is achieved, provided that the incoming information rate and the read-out rate to and from the nano-transceiver can match the channel rate. By increasing β, the single-user rate is reduced, but the requirements on the transceiver are greatly relaxed, as we explained in Sec. II. Analytically solving the maximum information rate expression given by (22) is not feasible. Instead, we numerically investigate it in Sec. VI.

V. Multi-user Achievable Information Rate in TS-OOK

In this section, we develop a stochastic model for interference in TS-OOK and formulate the multi-user achievable information rate analytically.

A. Stochastic Model of Multi-user Interference in TS-OOK

Multi-user interference in TS-OOK occurs when symbols from different nano-devices reach the receiver at the same time and overlap. Without loss of generality, we focus on the symbols transmitted by the nano-device number 1. Then, the interference I at the receiver j during the detection of a symbol from node number 1 is given by:

$$I = \sum_{u=2}^{U} A^u \left(p * h\right)^{u,j} \left(\mathcal{T}_1^u\right) + n^{u,j}\left(\mathcal{T}_1^u\right), \tag{24}$$

where U refers to the total number of nano-devices, A^u is the amplitude of the symbol transmitted by the nano-device u (either one or zero), $\left(p * h\right)^{u,j}$ stands for the transmitted pulse convoluted with the system impulse response between nano-devices u and j, $\mathcal{T}_1^u$ is the time difference at the receiver side between the transmissions from nano-devices 1 and u, and $n^{u,j}$ is the absorption noise created at the receiver by the transmissions from the nano-device u.

Many stochastic models of interference have been developed to date. For example, an extensive review of the existing models can be found in [38], [39], [40]. However, these models do not capture the peculiarities of the Terahertz Band channel, such as the molecular absorption loss and the additional molecular absorption noise created by interfering nodes. In order to provide a stochastic characterization of the interference in TS-OOK, we make the following considerations:

1) Nano-devices are not controlled by a central entity, but they communicate in an uncoordinated fashion.
2) Transmissions from different nano-devices are independent and follow the same source probability X.
3) The random initial time τ in (10) is uniformly distributed.
4) Nano-devices are uniformly distributed in space, thus, the propagation delay between any pair of nano-devices is also uniformly distributed in time.
5) Collisions between silences are not harmful. Collisions between pulses and silences are only harmful from the silence perspective.

Under these considerations, the time difference at the receiver side between the transmissions from the nano-devices 1 and u, $\mathcal{T}_1^u$, can be modeled as a uniform random variable over $[0, T_s]$. In addition, we can model the overall interference I as a Gaussian random process, $\mathcal{N}_I\left(\mu_I = E\left[I\right]; \sigma_I^2 = N_I\right)$, where $E\left[I\right]$ and N_I are the mean and variance of the interference, respectively. Indeed, for a single interfering nano-device, the amplitude of the interference depends on the propagation conditions and the distance between this user and the receiver. In addition, this interference can be constructive or destructive, depending on the phase of the pulses at the detector. Then, for a large number of users, we can invoke the Central Limit Theorem [37], and make the Gaussian assumption for I. We acknowledge that this assumption is mainly valid for very high nano-device density, larger than β in our analysis, which is what we would expect in applications such as WNSNs. We will consider nano-device densities of up to 10^6 nodes in a one-meter-radius disk centered at the receiver in our analysis.

The mean of the interference $E\left[I\right]$ is defined as:

$$\begin{aligned} E\left[I\right] &= E\left[\sum_{u=2}^{U} A^u \left(p * h\right)^{u,j}\left(\mathcal{T}_1^u\right) + n^{u,j}\left(\mathcal{T}_1^u\right)\right] \\ &= \sum_{u=2}^{U} \frac{T_p}{T_s} a^{u,j} p_X\left(x_1\right) = \sum_{u=2}^{U} \frac{a^{u,j}}{\beta} p_X\left(x_1\right), \end{aligned} \tag{25}$$

where U refers to the total number of nano-devices, T_p is the pulse length, T_s is the time between symbols, and $a^{u,j}$ is the average amplitude of a pulse at the receiver, j, transmitted by the nano-device u.

The variance of the interference is given by:

$$N_I = E\left[I^2\right] - E\left[I\right]^2, \tag{26}$$

where

$$\begin{aligned} E\left[I^2\right] &= E\left[\left(\sum_{u=2}^{U} A^u \left(p * h\right)^{u,j}\left(\mathcal{T}_1^u\right) + n^{u,j}\left(\mathcal{T}_1^u\right)\right)^2\right] \\ &= \sum_{u=2}^{U} \left(\frac{\left(a^{u,j}\right)^2 + N^{u,j}}{\beta}\right) p_X\left(x_1\right) \\ &\quad + 2\sum_{u=2<v}^{U} \left(\frac{p_X\left(x_1\right)}{\beta}\right)^2 a^{u,j} a^{v,j}, \end{aligned} \tag{27}$$

and which results in

$$\begin{aligned} N_I &= \sum_{u=2}^{U} \left(\frac{\left(a^{u,j}\right)^2 + N^{u,j}}{\beta}\right) p_X\left(x_1\right) \\ &\quad + 2\sum_{u=2<v}^{U} \left(\frac{p_X\left(x_1\right)}{\beta}\right)^2 a^{u,j} a^{v,j} - \left(\sum_{u=2}^{U} \frac{a^{u,j}}{\beta} p_X\left(x_1\right)\right)^2, \end{aligned} \tag{28}$$

where U is the total number of nano-devices, $a^{u,j}$ refers to the amplitude of the pulse transmitted by u at the receiver j, $N^{u,j}$ is the noise power created from the transmission from u to j, and $p_X\left(x_1\right)$ is the probability of transmitting a pulse.

B. Analytical Study of the Multi-user Information Rate

We define the multi-user achievable information rate as the maximum aggregated throughput that can be transmitted over the network, i.e.,

$$IR_{net} = \max_{X} \left\{ U \frac{B}{\beta} IR^{I}_{u-sym} \right\}, \tag{29}$$

where U refers to the number of interfering nano-devices, X refers to the source of information for every single nano-device, and IR^{I}_{u-sym} is the maximum achievable information rate for every single nano-device. Because of multi-user interference, IR^{I}_{u-sym} cannot be computed directly from (18). The optimal source distribution X depends on the number of interfering nano-devices in the network, U, and, thus, obtaining the multi-user maximum achievable information rate means to jointly optimize X and U.

In order to determine the IR^{I}_{u-sym} as a function of the number of nano-devices U, we need to add the contribution of interference into the probability of the output Y given the input $X = x_m$. Taking into account the previously introduced model for interference, now (21) becomes:

$$f^{I}_{Y}\left(Y|X = x_m\right) = \frac{1}{\sqrt{2\pi\left(N_m + N_I\right)}} e^{-\frac{1}{2}\frac{(y-E[I]-a_m)^2}{N_m+N_I}}, \tag{30}$$

where N_m stands for the noise power associated to the symbol m, N_I is variance of the interference, and $E[I]$ is the mean value of the interference. Then, IR^{I}_{u-sym} can be obtained by combining (30), (20) and (19) in (18). Finally, the multi-user achievable information rate is given by (31). Similarly to the single-user case, analytically solving this optimization problem is not feasible. For this, we numerically investigate it next.

VI. Numerical Results

In this section, we first validate our analytical model for the Terahertz Band channel time response. Then, we numerically analyze the performance of TS-OOK in the single-user case and the multi-user case.

A. COMSOL Validation of the System Impulse Response

We use COMSOL Multi-physics [18] to validate the antenna and Terahertz Band system impulse response. For this, we set-up a time-dependent transient electromagnetic simulation in COMSOL. A time domain analysis allows us to implicitly validate the system response over the entire frequency range of interest (from 100 GHz to 6 THz in this case). In addition, it allows us to validate the delay/phase of the received signals, and not just their amplitude or power. We use an isotropic electric point dipole as the EM source. The current density at the transmitting antenna corresponds to a one-hundred-femtosecond-long Gaussian pulse, whose maximum is centered at 800 fs. For this set of figures, we define several EM point probes at distances equal to 500 μm, 1 mm, 2.5 mm and 5 mm, respectively. The system response at larger distances is simulated in the same way at the cost of a higher computational complexity.

First, we focus on the analysis of the system response at a fixed distance. The system impulse response h at a distance $d = 1$ mm is illustrated in Fig. 2(a). We compare two different results. First, (8) is numerically evaluated in the case of having a joint antenna in transmission and in reception response that satisfies $\left|H^{T}_{ant} H^{R}_{ant}\right|^2 = \lambda_0^2/4\pi$, where $\lambda_0 = c/f_0$ and f_0 is the antenna design frequency and corresponds to the center frequency of the pulse p.s.d., approximately 1.6 THz. Second, the detected EM signal at a point probe at $d = 1$ mm in our COMSOL simulation is shown. We can observe that the analytical model can accurately reproduce the simulation results. The peak of the system impulse response corresponds to expected delay at 1 mm from the source. The amplitude of the major lobe of the system impulse response is the same in the two cases. The signal is affected by very small amplitude fluctuations due to the molecular absorption frequency selective behavior. However, there is a small discrepancy in the amplitude of the first secondary lobes in the system.

To better understand what is happening, we show in Fig. 2(b) the system frequency response. In this case, we can see that for frequencies above 1 THz, the analytical model given by (8) can match the simulation results. However, for lower frequencies, there is a mismatch between the analytical model and the simulation results. We associate this difference to the way in which the temporal response of an isotropic point dipole is modeled in COMSOL. Due to the fact that the p.s.d. of the transmitted signal x is mainly between 1 THz and 4 THz, this difference does not drastically affect our results.

In Fig. 2(c), the received signal at a distance $d = 1$ mm is

$$\begin{aligned} IR_{net} = \max_{X} \Bigg\{ U \frac{B}{\beta} \Bigg(& - \sum_{m=0}^{1} p_X\left(x_m\right) \log_2 p_X\left(x_m\right) - \int \sum_{m=0}^{1} \frac{1}{\sqrt{2\pi\left(N_m + N_I\right)}} e^{-\frac{1}{2}\frac{(y-E[I]-a_m)^2}{N_m+N_I}} p_X\left(x_m\right) \\ & \cdot \log_2 \left(\sum_{n=0}^{1} \frac{p_X\left(x_n\right)}{p_X\left(x_m\right)} \sqrt{\frac{N_m + N_I}{N_n + N_I}} e^{-\frac{1}{2}\frac{(y-E[I]-a_n)^2}{N_m+N_I} + \frac{1}{2}\frac{(y-E[I]-a_m)^2}{N_m+N_I}} \right) dy \Bigg) \Bigg\} \\ = - \max_{p_X(x_0)} \Bigg\{ U \frac{B}{\beta} \int & \frac{p_X\left(x_0\right)}{\sqrt{2\pi\left(N_0 + N_I\right)}} e^{-\frac{1}{2}\frac{(y-E[I])^2}{N_0+N_I}} \log_2 \left(p_X\left(x_0\right) \left(1 + \frac{1 - p_X\left(x_0\right)}{p_X\left(x_0\right)} \sqrt{\frac{N_0 + N_I}{N_1 + N_I}} e^{-\frac{1}{2}\frac{(y-E[I])^2}{N_0+N_I} + \frac{1}{2}\frac{(y-a_1-E[I])^2}{N_1+N_I}} \right) \right) \\ & + \frac{1 - p_X\left(x_0\right)}{\sqrt{2\pi\left(N_1 + N_I\right)}} e^{-\frac{1}{2}\frac{(y-a_1-E[I])^2}{N_1+N_I}} \log_2 \left(\left(1 - p_X\left(x_0\right)\right) \left(1 + \frac{p_X\left(x_0\right)}{1 - p_X\left(x_0\right)} \sqrt{\frac{N_1 + N_I}{N_0 + N_I}} e^{-\frac{1}{2}\frac{(y-a_1-E[I])^2}{N_1+N_I} + \frac{1}{2}\frac{(y-E[I])^2}{N_0+N_I}} \right) \right) dy \Bigg\} \end{aligned} \tag{31}$$

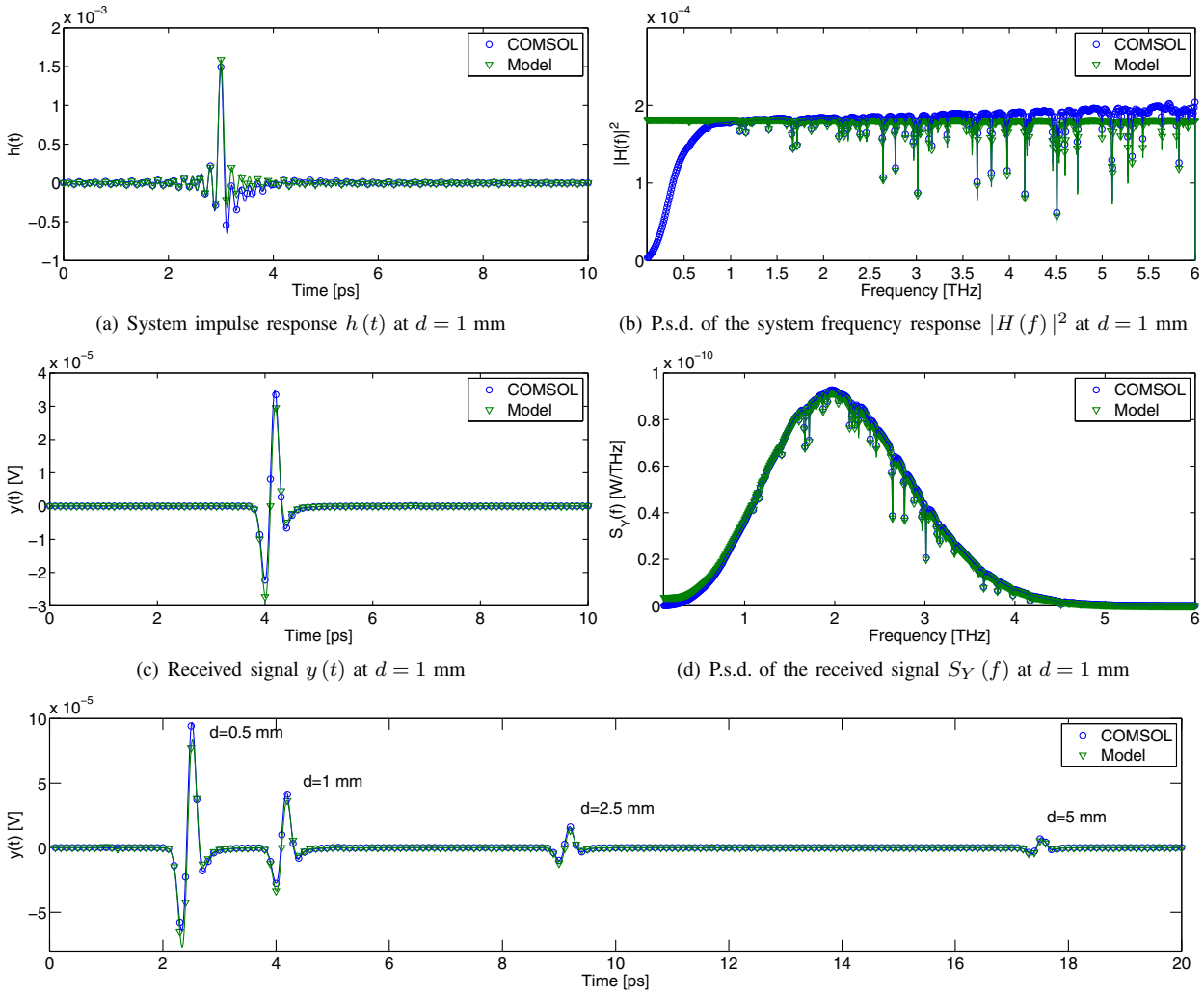

(a) System impulse response $h\,(t)$ at $d = 1$ mm

(b) P.s.d. of the system frequency response $|H\,(f)\,|^2$ at $d = 1$ mm

(c) Received signal $y\,(t)$ at $d = 1$ mm

(d) P.s.d. of the received signal $S_Y\,(f)$ at $d = 1$ mm

(e) Received signal $y\,(t)$ at different distances d.

Fig. 2. Terahertz Band system model validation with COMSOL Multi-physics.

illustrated. The received signal analytical model can accurately reproduce the results obtained in the COMSOL simulations. The delay in the maximum of the received signal perfectly matches in the two cases. The shape of the received pulses is also very similar. Once again, the differences originate in the impulse response of the electric point dipole used in COMSOL. This can be observed by comparing the p.s.d. of the received signal y, which is illustrated in Fig. 2(d). Finally, the distance dependence of the system impulse response is also validated, by analyzing the received signal at different distances. In Fig. 2(e), the received signal y at distances equal to 500 μm, 1 mm, 2.5 mm and 5 mm are shown, which further validates our analytical model. In the rest of the section, we use the system model to analyze the performance of TS-OOK.

B. Single-user Achievable Information Rate in TS-OOK

After the validation of the pulse propagation properties, we numerically investigate the maximum achievable information rate for TS-OOK in the single-user case.

1) Received Signal Power and Noise Power Ratios: First of all, it is convenient to visualize the behavior of the received pulse power and noise power with the distance. The received signal power P_1 when a pulse has been transmitted is shown in Fig. 3(a) as a function of the transmission distance d. In the same figure, the noise powers associated with the transmission of a pulse and the transmission of silence, N_1 and N_0, respectively, are also represented as functions of the transmission distance d. In particular,

- For distances below a few millimeters, the received pulse power P_1 is much larger than the power of the molecular absorption noise N_1.
- For longer transmission distances, the received signal power P_1 and the noise power N_1 generated by the transmitted pulse decrease, but the latter does so at a lower pace. More noise is generated as the signal propagates, but this is spread over a larger volume.
- The power N_0 associated with the transmission of silence is constant with distance and usually much smaller than N_1. This asymmetry in the noise behavior is the main difference with respect to the classical AWGN channel.

In Fig. 3(b), the signal to noise ratio when a pulse is transmitted $S_1 N_1 R = P_1/N_1$ and the pulse-noise-power to silence-noise-power ratio N_1/N_0 are shown as functions of d. These two ratios play a major role in the achievable information rate

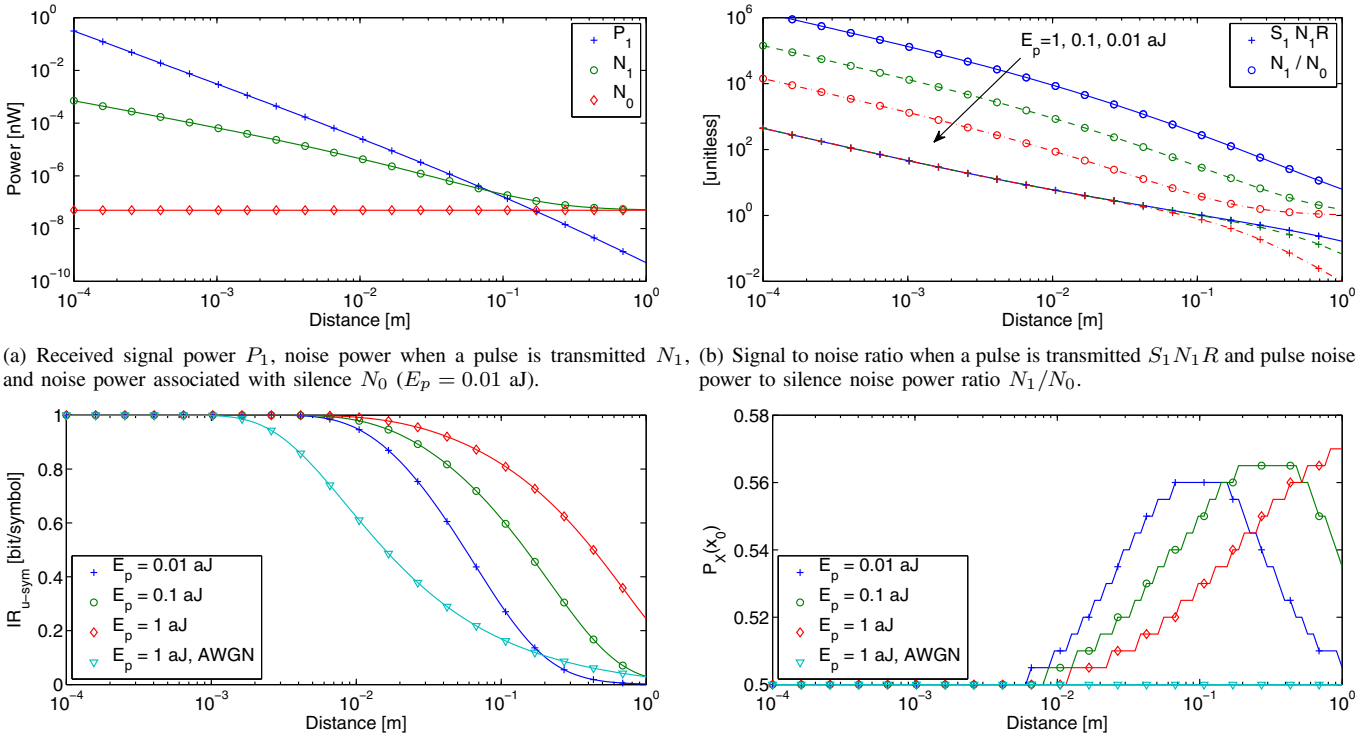

(a) Received signal power P_1, noise power when a pulse is transmitted N_1, and noise power associated with silence N_0 ($E_p = 0.01$ aJ).

(b) Signal to noise ratio when a pulse is transmitted $S_1 N_1 R$ and pulse noise power to silence noise power ratio N_1/N_0.

(c) Single-user information rate in bit/symbol for different noise power N_1 and N_0 ratios.

(d) Optimal probability to transmit a logical "0" for different noise power N_1 and N_0 ratios.

Fig. 3. Numerical analysis of the single-user achievable information rate in TS-OOK.

and the probability source distribution for which it is achieved, as we explain next.

2) Achievable Information Rate: The single-user maximum achievable information rate IR_{u-sym} in (22) in bit/symbol is shown in Fig. 3(c) as a function of the transmission distance d, for different values for the transmitted pulse energy E_p. Besides the Terahertz Band asymmetric noise model described in Sec. IV-A, we also evaluate the case in which the same noise power affects the transmission of pulses and of silences, as in the classical AWGN channel. The results are as follows:

- For transmission distances below a few millimeters, the information rate is almost constant and equal to 1 bit/symbol, which is the maximum information per symbol that can be transmitted in a binary system. For example, if $\beta = 1000$ and $B = 10$ THz, the single-user information rate is approximately 10 Gigabit/second. If $\beta = 10$, information rates in the order of 1 Terabit/second are possible. Ultimately, the achievable information rate is limited but the symbol generation rate and the maximum rate at which the electronics at the receiver side can process the received signals. The use of graphene and other very high-electron-mobility materials, will enable the processing at speeds up to a few Terabits per second, thus, making the most out of the Terahertz Band channel.
- As the transmission distance increases, the achievable information rate decreases, but it does so at a lower pace than in the case of the symmetric additive Gaussian noise channel. This phenomenon can be explained as follows. When the transmission distance increases, the received signal power P_1 associated with the transmission of a pulse and the noise power N_1 created by the propagation of this pulse become comparable and, thus, the pulse to noise ratio, $S_1 N_1 R$, tends to one. However, as long as the total signal power received is higher than the background noise level N_0, the receiver can still distinguish between a transmission and a no-transmission, because the p.d.f.s of the two signals are largely different.
- When the transmission distance further increases, the noise power N_1 tends to N_0, and thus, the achievable information rate tends to zero because the symbols cannot be distinguished, as expected.

3) Optimal Source Probability Distribution: The asymmetric behavior of the Terahertz channel is also reflected on the optimal source probability distribution X for which the maximum achievable information rate is achieved. The optimal probability to transmit a logical "0" $p_X(X_0)$ for which the maximum rate is achieved is shown in Fig. 3(d) as a function of the transmission distance d for different values of the pulse-noise-power to silence-noise-power ratio N_1/N_0. In particular,

- For transmission distances below a few millimeters, the optimal source probability distribution corresponds to the binary equiprobable distribution ($p_X(x_0) = p_X(x_1) = 0.5$), as in the symmetric AWGN channel.
- When the transmission distance increases, even if both silence and pulses can be easily detected, the optimal probability distribution is no longer the equiprobable one, but one that favors the transmission of silence rather than pulses, because the total noise or equivocation is much lower when zeros are transmitted. In particular, $p_X(x_0)$ approaches 0.55 for distances above 10 mm.

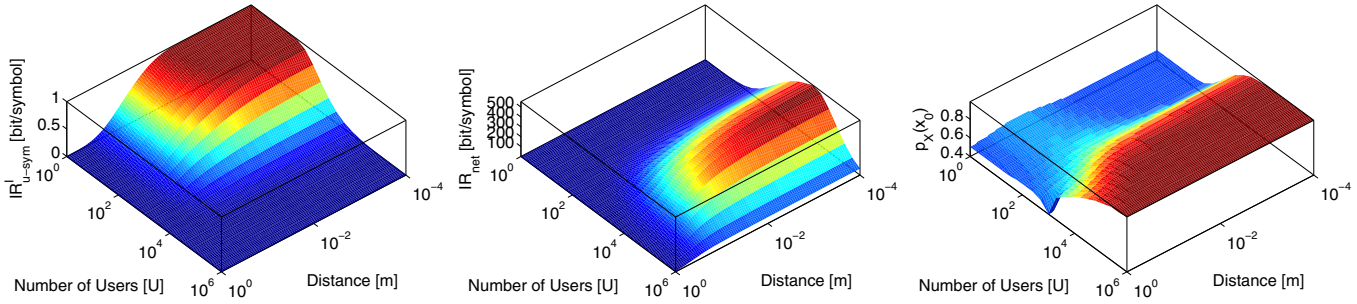

(a) Single-user achievable information rate for every single nano-device.

(b) Aggregated multi-user achievable information rate.

(c) Optimal probability to transmit a logical "0".

Fig. 4. Numerical analysis of the multi-user achievable information rate in TS-OOK.

Ultimately, these results motivate the development of channel coding schemes in which more zeros than ones are used. At the same time, by utilizing codes that make the transmitter to stay silent for long periods of time can compromise the synchronization needed between transmitter and receiver. For the time being, synchronization schemes for ultra-broadband pulse-based communications in the Terahertz Band do not exist, and will be developed as part of our future work.

C. Multi-user Achievable Information Rate in TS-OOK

In this section, we quantitatively study the effects of interference on the achievable information rate of a single user and on the aggregated throughput. The energy of a transmitted pulse is kept constant and equal to 0.01 aJ. The ratio between the time between pulses and the pulse duration is kept constant and equal to $\beta = 1000$. For the computation of the interference, we consider the neighboring nodes to be uniformly distributed in a 1-meter radius disk centered at the receiver.

1) Single-user Achievable Information Rate with Multi-user Interference: In Fig. 4(a), the achievable information rate for every nano-device IR^I_{u-sym} in bit/symbol, obtained from (18), (19) and (20) in (30), is shown as a function of the number of nano-devices U and the transmission distance d. The results show that

- For a low number of interfering nano-devices, the achievable information rate behaves with distance similarly to the single-user case studied in Sec. VI-B.
- As the number of interfering nano-devices increases, the total interference becomes the dominant term in the equivocation of the channel. As a result, the achievable information rate of every user tends to zero. Interference affects in the same way the reception of noise and the reception of pulses and, thus, once it becomes the dominant contribution to the received signal, the achievable information rate degrades quickly.

2) Multi-user Achievable Information Rate and Optimal Source Probability Distribution: The multi-user achievable information rate IR_{net} in (31) as a function of the number of interfering nano-devices U and the transmission distance d is shown in Fig. 4(b). Different trends for the multi-user achievable information rate can be observed depending on the transmission distance and the number of nano-devices. To understand this behavior, it is important to identify which is the optimal source probability distribution X for which the multi-user achievable information rate is achieved. In Fig. 4(c), the optimal probability to transmit a logical "0" $p_X(x_0)$, for which the single-user achievable information rate and the aggregated multi-user achievable information rate are achieved, is shown as a function of the number of nano-devices U and the transmission distance d.

In the multi-user scenario, *the optimal source distribution clearly prioritizes the transmission of logical "0"s or silence over logical "1"s or pulses*, i.e., $p_X(x_0) \gg p_X(x_1)$. This is due to the fact that by transmitting silence, both the molecular absorption noise and especially the interference power are drastically reduced. Indeed, this result is just numerically stating that collisions between silence are never harmful, and, thus, it is more convenient for the entire network to minimize the number of pulses that are sent. This behavior is not seen in PAM or PPM modulations, where the information is modulated in the shape or the position of the pulses, and pulses are always transmitted. In TS-OOK, *the information is ultimately placed in the presence or absence of "signal"* (in this case a pulse due to technology limitations, but could be just any signal shape or even noise). This result motivates the development of channel coding schemes suited for nano-devices and which maximize the number of logical "0"s. At the same time, by transmitting less pulses, the total energy consumption for every device is also reduced. However, the transmission of sequences with a very large number of "0"s might hamper the synchronization among the transmitting and the receiving nano-devices. Finally, for the highest node densities, the Gaussian approximation might not hold any longer, due to the fact that the probability to transmit a pulse tends to 0 and thus, the interference tends to 0. However, the utilized model is sufficient to illustrate the trends in the achievable rates.

We can now explain the behavior of the multi-user achievable information rate for the different transmission distances:

- When the transmission distance is short, below a few tens of millimeters, the multi-user achievable information rate increases with the number U of nano-devices up to a point at which it reaches a constant value. This effect appears because, even when the number of interfering nano-devices is drastically increased, provided that the individual probability to transmit silence is much higher than the probability to transmit a pulse ($p_X(x_0) \gg$

$p_X(x_1)$), the total interference does not increase at the same pace. Thus, the received signal power is sufficiently large to be distinguishable from the reception of silence.

- When the transmission distance is increased, even by transmitting primarily silence, the power of the received signal when a pulse is transmitted diminishes very fast because of the very high path-loss of the Terahertz Band, and it is very difficult for the receiver to discern between pulses and silence. It is interesting to note that, for transmission distances above a few tens of millimeters, there is an optimal number of users for which the multi-user achievable information rate is maximum. The optimal point is again related to the relation between the transmitted and received pulse energy and the total interference power.

VII. Conclusions

Wireless communication among nano-devices will boost the applications of nanotechnology in many fields of our society, ranging from healthcare to homeland security and environmental protection. However, enabling the communication among nano-devices is still an unsolved challenge. In this paper, we presented a modulation and channel access scheme for nano-devices, which is based on the exchange of femtosecond-long pulses by following an on-off keying modulation spread in time. We studied the performance of this new paradigm analytically and provided numerical solutions to the maximal achievable information rate for the single-user and the multi-user cases. We developed analytical models for the path-loss, molecular absorption noise and interference in the Terahertz Band, which is the expected frequency range of operation of novel plasmonic nano-antennas and nano-transceivers. These models have been validated by means of extensive time-domain electromagnetic simulations with COMSOL.

The results show that the proposed modulation can support a very large number of nano-devices simultaneously transmitting at multiple Gigabits-per-second and up to Terabits-per-second, depending on the modulation parameters and the network conditions and given that asymmetric channel coding schemes are used to prioritize the transmission of silence. Indeed, both the maximum single-user and multi-user information rates are achieved when asymmetric source probability distributions are used, contrary to the classical symmetric AWGN channel. This study stimulates discussion and further research on synchronization, channel coding and medium access for nanonetworks.

References

[1] J. M. Jornet and I. F. Akyildiz, "Information capacity of pulse-based wireless nanosensor networks," in *Proc. 2011 IEEE Communications Society Conference on Sensor, Mesh and Ad Hoc Communications and Networks.*

[2] I. F. Akyildiz and J. M. Jornet, "Electromagnetic wireless nanosensor networks," *Nano Commun. Networks J.*, vol. 1, no. 1, pp. 3–19, Mar. 2010.

[3] S. Abadal, E. Alarcon, A. Cabellos-Aparicio, M. Lemme, and M. Nemirovsky, "Graphene-enabled wireless communication for massive multicore architectures," *IEEE Commun. Mag.*, vol. 51, no. 11, pp. 137–143, 2013.

[4] A. K. Geim and K. S. Novoselov, "The rise of graphene," *Nature Materials*, vol. 6, no. 3, pp. 183–191, Mar. 2007.

[5] M. Tamagnone, J. S. Gomez-Diaz, J. R. Mosig, and J. Perruisseau-Carrier, "Reconfigurable terahertz plasmonic antenna concept using a graphene stack," *Applied Physics Lett.*, vol. 101, no. 21, p. 214102, 2012.

[6] J. M. Jornet and I. F. Akyildiz, "Graphene-based plasmonic nano-antenna for terahertz band communication in nanonetworks," *IEEE J. Sel. Areas Commun.*, vol. 12, no. 12, pp. 685–694, Dec. 2013.

[7] H. Song and T. Nagatsuma, "Present and future of terahertz communications," *IEEE Trans. Terahertz Science and Technol.*, 2011.

[8] T. Kurner and S. Priebe, "Towards THz communications-status in research, standardization and regulation," *J. Infrared, Millimeter, and Terahertz Waves*, vol. 35, no. 1, pp. 53–62, 2014.

[9] I. F. Akyildiz, J. M. Jornet, and C. Han, "Terahertz band: next frontier for wireless communications," *Physical Commun. J.*, vol. 12, pp. 16–32, Sep. 2014.

[10] W. Knap, F. Teppe, N. Dyakonova, D. Coquillat, and J. Lusakowski, "Plasma wave oscillations in nanometer field effect transistors for terahertz detection and emission," *J. Physics: Condensed Matter*, vol. 20, no. 38, p. 384205, 2008.

[11] L. Vicarelli, M. S. Vitiello, D. Coquillat, A. Lombardo, A. C. Ferrari, W. Knap, M. Polini, V. Pellegrini, and A. Tredicucci, "Graphene field-effect transistors as room-temperature terahertz detectors," *Nature Materials*, vol. 11, pp. 865–871, Oct. 2012.

[12] M. C. Wanke, M. Lee, C. D. Nordquist, M. J. Cich, M. Cavaliere, A. M. Rowen, J. R. Gillen, C. L. Arrington, A. D. Grine, C. T. Fuller, and J. L. Reno, "Integrated chip-scale thz technology," *Proc. SPIE*, pp. 80 310E–80 310E–10, 2011.

[13] H.-J. Song, K. Ajito, Y. Muramoto, A. Wakatsuki, T. Nagatsuma, and N. Kukutsu, "24 gbit/s data transmission in 300 GHz band for future terahertz communications," *Electron. Lett.*, vol. 48, no. 1, pp. 953–954, July 2012.

[14] C. Wang, C. Lin, Q. Chen, B. Lu, X. Deng, and J. Zhang, "A 10-gbit/s wireless communication link using 16-QAM modulation in 140-GHz band," *IEEE Trans. Microwave Theory and Techniques*, vol. 61, no. 7, pp. 2737–2746, July 2013.

[15] S. Koenig, D. Lopez-Diaz, J. Antes, F. Boes, R. Henneberger, A. Leuther, A. Tessmann, R. Schmogrow, D. Hillerkuss, R. Palmer, *et al.*, "Wireless sub-THz communication system with high data rate," *Nature Photonics*, vol. 7, no. 12, pp. 977–981, 2013.

[16] M. Win and R. Scholtz, "Ultra-wide bandwidth time-hopping spread-spectrum impulse radio for wireless multiple-access communications," *IEEE Trans. Commun.*, vol. 48, no. 4, pp. 679–689, 2000.

[17] W. Brown, B. Wallin, D. Lesniewski, D. Gooding, and J. Martin, "The experimental determination of on-off keying laser communications probability models and a comparison with theory," *Proc.*, pp. 61 050U–61 050U–8, 2006.

[18] COMSOL Multiphysics Simulation Software. COMSOL. Available: http://www.comsol.com/products/multiphysics/

[19] Q. Gu, Z. Xu, H.-Y. Jian, B. Pan, X. Xu, M.-C. Chang, W. Liu, and H. Fetterman, "CMOS THz generator with frequency selective negative resistance tank," *IEEE Trans. Terahertz Sci. and Technol.*, vol. 2, no. 2, pp. 193–202, 2012.

[20] E. Ojefors, B. Heinemann, and U. Pfeiffer, "Subharmonic 220-and 320-GHz SiGe HBT receiver front-ends," *IEEE Trans. Microwave Theory and Techniques*, vol. 60, no. 5, pp. 1397–1404, 2012.

[21] V. Radisic, K. Leong, X. Mei, S. Sarkozy, W. Yoshida, and W. Deal, "Power amplification at 0.65 THz using InP HEMTs," *IEEE Trans. Microwave Theory and Techniques*, vol. 60, no. 3, pp. 724–729, 2012.

[22] K. Shinohara, D. Regan, Y. Tang, A. Corrion, D. Brown, J. Wong, J. Robinson, H. Fung, A. Schmitz, T. Oh, S. Kim, P. Chen, R. Nagele, A. Margomenos, and M. Micovic, "Scaling of GaN HEMTs and Schottky diodes for submillimeter-wave MMIC applications," *IEEE Trans. Electron. Devices*, vol. 60, no. 10, pp. 2982–2996, 2013.

[23] D. Woolard, P. Zhao, C. Rutherglen, Z. Yu, P. Burke, S. Brueck, and A. Stintz, "Nanoscale imaging technology for THz-frequency transmission microscopy," *International J. High Speed Electron. and Systems*, vol. 18, no. 1, pp. 205–222, 2008.

[24] A. Shlivinski, E. Heyman, and R. Kastner, "Antenna characterization in the time domain," *IEEE Trans. Antennas Propag.*, vol. 45, no. 7, pp. 1140–1149, 1997.

[25] A. E. C. Tan, M. Y. W. Chia, K. K. M. Chan, and K. Rambabu, "Modeling the transient radiated and received pulses of ultra-wideband antennas," *IEEE Trans. Antennas Propag.*, vol. 61, no. 1, pp. 338–345, 2013.

[26] K. Yasuko and S. Takamasa, "Terahertz-wave propagation model," *J. of the National Institute of Inf. and Commun. Technol.*, vol. 55, no. 1, pp. 73–77, 2008.

[27] T. Kleine-Ostmann, C. Jastrow, S. Priebe, M. Jacob, T. Kurner, and T. Schrader, "Measurement of channel and propagation properties at 300 GHz," in *Proc. 2012 Conference on Precision Electromagnetic Measurements*, pp. 258–259.
[28] S. Priebe and T. Kurner, "Stochastic modeling of thz indoor radio channels," *IEEE Trans. Wireless Commun.*, vol. 12, no. 9, pp. 4445–4455, 2013.
[29] J. M. Jornet and I. F. Akyildiz, "Channel modeling and capacity analysis of electromagnetic wireless nanonetworks in the terahertz band," *IEEE Trans. Wireless Commun.*, vol. 10, no. 10, pp. 3211–3221, Oct. 2011.
[30] C. Jansen, S. Priebe, C. Moller, M. Jacob, H. Dierke, M. Koch, and T. Kurner, "Diffuse scattering from rough surfaces in thz communication channels," *IEEE Trans. Terahertz Sci. and Technol.*, vol. 1, no. 2, pp. 462–472, 2011.
[31] J. W. Song, G. R. Aizin, J. Mikalopas, Y. Kawano, K. Ishibashi, N. Aoki, J. L. Reno, Y. Ochiai, and J. P. Bird, "Bolometric terahertz detection in pinched-off quantum point contacts," *Applied Physics Lett.*, vol. 97, no. 8, p. 083109, 2010.
[32] F. Sizov and A. Rogalski, "THz detectors," *Progress in Quantum Electron.*, vol. 34, no. 5, pp. 278–347, 2010.
[33] V. Y. Kachorovskii, S. L. Rumyantsev, W. Knap, and M. Shur, "Performance limits for field effect transistors as terahertz detectors," *Applied Physics Lett.*, vol. 102, no. 22, 2013.
[34] R. G. Cid-Fuentes, J. M. Jornet, E. Alarcon, and I. F. Akyildiz, "A receiver architecture for pulse-based electromagnetic nanonetworks in the terahertz band," in *Proc. 2012 IEEE International Conference on Communications.*
[35] F. Box, "Utilization of atmospheric transmission losses for interference-resistant communications," *IEEE Trans. Commun.*, vol. 34, no. 10, pp. 1009–1015, Oct. 1986.
[36] R. M. Goody and Y. L. Yung, *Atmospheric Radiation: Theoretical Basis*, 2nd ed. Oxford University Press, 1989.
[37] A. Papoulis and S. U. Pillai, *Probability, Random Variables and Stochastic Processes*. McGraw-Hill, 2002.
[38] P. Cardieri, "Modeling interference in wireless ad hoc networks," *IEEE Commun. Surveys and Tutorials*, vol. 12, no. 4, pp. 551–572, 2010.
[39] J. Andrews, R. Ganti, M. Haenggi, N. Jindal, and S. Weber, "A primer on spatial modeling and analysis in wireless networks," *IEEE Commun. Mag.*, vol. 48, no. 11, pp. 156–163, Nov. 2010.
[40] M. Win, P. Pinto, and L. Shepp, "A mathematical theory of network interference and its applications," *Proc. IEEE*, vol. 97, no. 2, pp. 205–230, Feb. 2009.

Josep Miquel Jornet received the Engineering Degree in Telecommunication and the Master of Science in Information and Communication Technologies from the Universitat Politecnica de Catalunya, Barcelona, Spain, in 2008. He received the Ph.D. degree in Electrical and Computer Engineering from the Georgia Institute of Technology, Atlanta, GA, in 2013, with a fellowship from "la Caixa" (2009-2010) and Fundacion Caja Madrid (2011-2012). He is currently an Assistant Professor with the Department of Electrical Engineering at the State University of New York (SUNY) at Buffalo. From September 2007 to December 2008, he was a visiting researcher at the Massachusetts Institute of Technology (MIT), Cambridge, under the MIT Sea Grant program. He was the recipient of the Oscar P. Cleaver Award for outstanding graduate students in the School of Electrical and Computer Engineering, at the Georgia Institute of Technology in 2009. He also received the Broadband Wireless Networking Lab Researcher of the Year Award at the Georgia Institute of Technology in 2010. He is a member of the IEEE and the ACM. His current research interests are in electromagnetic nanonetworks, graphene-enabled wireless communication, Terahertz Band communication networks and the Internet of Nano-Things.

Ian F. Akyildiz received the B.S., M.S., and Ph.D. degrees in Computer Engineering from the University of Erlangen-Nurnberg, Germany, in 1978, 1981 and 1984, respectively. Currently, he is the Ken Byers Chair Professor in Telecommunications with the School of Electrical and Computer Engineering, Georgia Institute of Technology, Atlanta, the Director of the Broadband Wireless Networking (BWN) Laboratory and the Chair of the Telecommunication Group at Georgia Tech. Since 2013, he is a FiDiPro Professor (Finland Distinguished Professor Program (FiDiPro) supported by the Academy of Finland) in the Department of Electronics and Communications Engineering, at Tampere University of Technology, Finland, and the founding director of NCC (Nano Communications Center). Since 2008, he is also an honorary professor with the School of Electrical Engineering at Universitat Politecnica de Catalunya (UPC) in Barcelona, Catalunya, Spain and the founding director of N3Cat (NaNoNetworking Center in Catalunya). Since 2011, he is a Consulting Chair Professor at the Department of Information Technology, King Abdulaziz University (KAU) in Jeddah, Saudi Arabia. He is the Editor-in-Chief of *Computer Networks* (Elsevier) Journal, and the founding Editor-in-Chief of the *Ad Hoc Networks* (Elsevier) Journal, the *Physical Communication* (Elsevier) Journal and the *Nano Communication Networks* (Elsevier) Journal. He is an IEEE Fellow (1996) and an ACM Fellow (1997). He received numerous awards from IEEE and ACM. His current research interests are in nanonetworks, Terahertz Band communication networks, Long Term Evolution Advanced (LTE-A) networks, cognitive radio networks and wireless sensor networks.